THE JOURNAL OF PHYSICAL CHEMISTRY C
A JOURNAL OF THE AMERICAN CHEMICAL SOCIETY

pubs.acs.org/JPCC

Article

Investigating Energy-Transfer Interactions in Perovskite Quantum Dot−Dye Assemblies

Selin E. Donmez, Sisi Wang, Unaisah Vorajee, Geoffrey F. Strouse, and Hedi Mattoussi*

Cite This: J. Phys. Chem. C 2025, 129, 4134−4145

Read Online

ACCESS | Metrics & More | Article Recommendations | Supporting Information

ABSTRACT: Colloidal quantum dots (QDs) exhibit several advantageous photophysical properties combined with a high surface-to-volume ratio, making them very attractive for use in processes relying on energy-transfer (ET) interactions. We have tested the effectiveness of $CsPbBr_3$ perovskite quantum dots (PQDs) as energy-transfer donors in hybrid PQD−dye assemblies. We combined PQDs and various cyanine dye molecules that present zwitterionic moieties and/or salt groups to promote tailored binding via electrostatic interactions and control the spectral overlap in PQD−dye pairs. This enabled the manipulation of the donor−acceptor stoichiometry of the assemblies. Using steady-state and time-resolved fluorescence spectroscopy, we evaluated the impact of varying the dye structure, photophysical characteristics, and dye-to-PQD ratio on the fluorescence properties of these hybrid conjugates. We find that the fluorescence quenching efficiency measured for these assemblies depends on key parameters, such as spectral overlap and number of dyes per assembly (or valence). Thorough analysis of our results indicates that invoking the Förster dipole−dipole and Dexter charge-transfer interaction mechanisms provides the best interpretation of the energy-transfer interaction in these donor−acceptor assemblies.

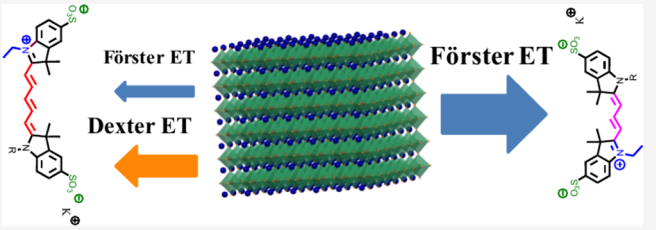

INTRODUCTION

Fluorescence resonance energy transfer, FRET, has for decades generated much interest as a fundamental photophysical phenomenon.[1,2] It has also found applications in many scientific areas such as physics, chemistry, biology, and engineering.[3−6] FRET between distinct dyes that are either tethered to the ends of a biomolecule or attached to individual molecules brought in close proximity has been used by researchers as a tool to probe a variety of biophysical processes.[1] Examples include changes in protein or a synthetic polymer conformation in response to external stimuli, protein−protein interactions, and ligand−receptor binding.[1−3]

FRET-based investigations have routinely employed organic fluorophores as donor and acceptor molecules.[1] However, these compounds have faced inherent photophysical limitations, such as broad emission peaks with red tailing, small spectral differences between absorption and emission profiles, and relatively narrow absorption windows. These features can significantly complicate spectral deconvolution and data analysis, which has limited the efficacy of FRET as an analytical tool in sensing and bioimaging applications.[7] The development of bottom-up, solution-phase growth of highly fluorescent and colloidally stable metal chalcogenide semiconductor quantum dots (QDs) has provided the community with new fluorophores that exhibit unique optical and spectroscopic characteristics that can improve FRET effectiveness and its use in various sensing applications.[8−17] Some of these advantages include size-dependent properties resulting from carrier quantum confinement, including narrow photoemission spectra, broad absorption profiles, and enhanced quantum yield achieved through surface passivation strategies.[18,19] Several studies investigating QD-based FRET have been reported over the past two decades.[18,20−26] A large fraction of those studies employed QDs as energy donors interacting with organic dye acceptors.[18,19,25,27] However, the use of QDs as acceptors was limited to FRET between differently sized QDs in close-packed films or QDs interacting with lanthanide−chelate donors.[24,28−32] In the latter, energy transfer (ET) was characterized using time-gated fluorescence measurements, which exploit the rather long exciton lifetime of the lanthanide to circumvent the efficient direct excitation of the QDs by acquiring the FRET-induced emission after several microseconds when the nanocrystal excitation has completely decayed (~10−20 ns).[28]

More recently, the success in preparing colloidal cesium lead halide perovskite nanocrystals made of $CsPbX_3$ (where X = chloride, bromide, or iodide) has added a new set of dispersible fluorescent materials, referred to as perovskite QDs (PQDs).[33−35] These materials have generated great interest, motivated by their photophysical attributes, including

Received: January 15, 2025
Revised: January 25, 2025
Accepted: January 28, 2025
Published: February 18, 2025

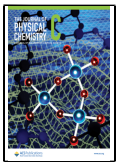

high photoluminescence quantum yield (PLQY) coupled with size- and composition-tunable narrow emission profiles. Owing to these characteristics, perovskite materials hold significant promise for various optoelectronic applications, including solar cell technology and light-emitting diodes.[36−39] PQDs are also tolerant to structural defects because energy traps tend to be shallow compared to conventional QDs.[35]

The broad light absorption and high PLQY exhibited by PQDs make them promising fluorophores that can enhance nonradiative energy-transfer interactions. For instance, Davis and co-workers have investigated the use of perylene-diimides (PDIs) as surface ligands and acceptor fluorophores interacting with $CsPbBr_3$ PQDs. In particular, they showed that mixing as-grown nanocrystals with carboxyl-functionalized PDI promotes enhanced emission by red and orange perylene diimide dye ligands through energy-transfer interactions.[40] Kamat and co-workers have characterized the excited-state interactions between $CsPbBr_3$ PQDs and RhB dyes and reported among others findings that they follow the dipole−dipole FRET interaction formalism.[41] In a recent study, Kovalenko and co-workers investigated energy-transfer interactions between $CsPbBr_3$ QDs and Cy3-NHS ester dyes at the single-molecule level.[42] They also reported data that exhibit characteristic dependencies on the spectral overlap.

In this study, we investigate the effectiveness of PQDs as ET donors in hybrid PQD−dye assemblies. We utilize cyanine (Cy3 and Cy5) dyes bearing zwitterionic moieties and/or salt groups as acceptor molecules that are brought in close proximity to the PQD surfaces by electrostatic interactions. We analyze the effects of varying the dye structure, photophysical characteristics, and valence on the fluorescence properties of these hybrid assemblies. Strong energy-transfer interactions have been measured using steady-state and time-resolved fluorescence experiments. Estimates of the transfer rates extracted from the data were compared to the predictions of the Förster dipole−dipole formalism. We find that the Förster model accounts well for the experimental data acquired for the PQD−Cy3 pair with a strong spectral overlap. However, a combination of dipole−dipole coupling and charge-transfer interactions invoked in the Dexter model is required to account for the data measured for the smaller spectral overlap PQD−Cy5 pair.

EXPERIMENTAL SECTION/MATERIALS AND METHODS

Growth of $CsPbBr_3$ Nanocrystals. The colloidal $CsPbBr_3$ PQDs used in this study were prepared under high-temperature reaction conditions, originally introduced by Kovalenko and co-workers.[43] A few minor adjustments were introduced to allow a larger-scale reaction to be implemented.[44] A stock solution of Cs-oleate precursor was first prepared by mixing 0.814 g (2.50 mmol) of Cs_2CO_3, 2.50 mL (7.90 mmol) of oleic acid (OA), and 40 mL of octadecene (ODE) in a 50 mL three-necked round-bottomed flask equipped with a stir bar. The mixture was degassed under vacuum for 1 h at 120 °C, and then the atmosphere was switched to nitrogen and the content was further heated to 150 °C, yielding a clear solution of Cs-oleate (after ∼30 min). The prepared Cs-oleate was stored under a nitrogen atmosphere at room temperature. In a separate 50 mL three-necked, round-bottomed flask equipped with a stir bar, 0.200 g (0.545 mmol) of $PbBr_2$ salt, 1.50 mL of OA, and 1.50 mL of OLA were mixed with 15 mL of ODE, heated to 120 °C, and degassed under vacuum for 30 min. The atmosphere was then switched to nitrogen, and the content was further heated to 160 °C until the $PbBr_2$ salt was dissolved. Then, 1.20 mL of the above Cs-oleate solution was rapidly injected into a flask containing the $PbBr_2$ mixture to initiate the growth of $CsPbBr_3$ nanocrystals. After 5 s of stirring, the flask was immersed in an ice bath to quench the growth, yielding a bright-green dispersion of nanocrystals. The dispersion was subjected to one round of centrifugation at 3500 rpm for 5 min. The supernatant containing ODE, byproducts, and excess ligands was discarded, and the green pellet was dispersed with sonication in 5 mL of hexane. One additional round of centrifugation for 5 min was applied, collecting the clear supernatant. A stock dispersion of nanocrystals with an adjusted final molar concentration of ∼5 μM was prepared by adding hexane and then stored until further use.[45] TEM characterization of the PQD sample indicated that the nanocrystals are cubic in shape with an edge size of 8.2 + 2.1 nm (see Figure S1)

Ligand Exchange and Phase Transfer. The sulfocyanine dyes used in this investigation are soluble in polar media, e.g., ethanol and water. However, the as-grown OA/OLA-PQDs exhibit severe colloidal and structural instability when exposed to polar media, a problem that arises from the ionic nature of the nanocrystal cores and dynamic binding of surface ligands.[35,46] One common approach for addressing nanocrystal instability is to substitute the native coating with higher-affinity ligands capable of endowing colloidal stability and enhanced passivation of the nanocrystal surfaces. We recently introduced a set of polyzwitterionic and polysalt polymer ligands that can simultaneously interact with cations and anions alike on the PQD surfaces. These ligands were shown to be effective in enabling the colloidal and structural stabilization of $CsPbBr_3$ PQDs in polar solvents such as ethanol for extended storage periods, making them ideally suitable for testing FRET interactions with our sulfo-cyanine dyes.[44,45] Ligand exchange of the as-grown PQDs with the zwitterion-rich polysulfobetaine polymer (polySB) and phase transfer to ethanol was performed following the steps described in reference 45. Briefly, in a 7 mL scintillation vial, 200 μL of OLA/OA-capped $CsPbBr_3$ PQDs in hexane was mixed with 6 mg of polySB dissolved in 400 μL of THF (prepared using an Eppendorf tube). After mixing for ∼1 min, the PQDs were precipitated by adding 3 mL of hexane. After sonication for ∼30 s, the mixture was centrifuged at 3500 rpm for 5 min. The clear supernatant was discarded, and the green pellet was redispersed in THF (200 μL), followed by another round of precipitation using excess hexane and centrifugation at 3500 rpm for 5 min. The resulting polySB-capped PQD powder was dispersed in anhydrous ethanol. More details about the polymer synthesis and characterization are provided in the Supporting Information and reference 45.

Assembly of PQD−Dye Conjugates. The samples used to probe the energy-transfer interactions between $CsPbBr_3$ PQDs and various cyanine dyes were prepared by mixing the nanocrystals dispersed in ethanol with varying molar amounts of the selected dye dissolved in ethanol. We first prepared stock samples of QD dispersions and dye solutions with a given molar concentration of each; these values were extracted from the UV−vis absorption data and using the molar absorption coefficients of the PQDs and dyes reported in the literature:[46] ε_{400} ($CsPbBr_3$ PQDs) = 6.65 μM^{-1} cm^{-1}, ε_{555} (Cy3−maleimide) = 150,000 cm^{-1} M^{-1}, ε_{648} (Cy5−maleimide) = 250,000 cm^{-1} M^{-1}, and ε_{555} (Cy3−NHS) =

https://doi.org/10.1021/acs.jpcc.5c00337
J. Phys. Chem. C 2025, 129, 4134−4145

150,000 cm^{-1} M^{-1}. When preparing the various PQD-plus-dye mixtures, the volumes of the stock PQD dispersion and dye solution were adjusted to yield samples with a fixed PQD molar concentration [PQD] of ∼120 nM, while the dye concentration was varied over the range of 0.3−14 μM. A few additional samples with [PQD] = 60 or 190 nM were also prepared and tested.

Dispersions of the hybrid assemblies were loaded onto a fluorescence quartz cuvette with a 5 mm optical path and a volume of ∼1 mL. The fluorescence spectra were acquired from the various samples using a narrow excitation line at 365 nm, where the dyes have minimal absorption, thus reducing the effects of the direct excitation contribution. Additionally, control spectra collected from solutions of the dye only were recorded and subtracted from the sample spectra to remove the dye contribution generated from direct excitation. To avoid inner filtering effects, PQD dispersions with an optical density (OD) at the excitation line below 0.5 were used for our measurements.

RESULTS AND DISCUSSION

Rationale. In this study, we aim to probe and understand the process of nonradiative energy-transfer interactions between all-inorganic $CsPbBr_3$ PQDs and conventional dye acceptors using a configuration that permits spatial proximity between the fluorophores and additionally allows control over the dye-to-PQD molar ratio (or hybrid conjugate valence). For this, we performed ligand substitution of the as-grown OA/OLA-stabilized PQDs with a multicoordinating polyzwitterion polymer presenting several sulfobetaine motifs along its backbone. We have previously demonstrated the capacity of this polymer to readily transfer $CsPbBr_3$ PQDs to several polar solvents including ethanol while promoting great long-term colloidal stability and preserving the high PL quantum yield of the nanocrystals.[45] Three cyanine dyes were used, one presenting an ammonium salt derivative (Cy3−NHS−ester) and the other two having a charge-balanced zwitterion group along with a potassium sulfonate salt (sulfo−Cy3−Mal and sulfo−Cy5−Mal). These dyes are expected to interact with the ionic PQD surfaces via electrostatic coupling, although binding is expected to be much stronger for sulfo−dye−Mal.

We evaluate the effectiveness of two models, the dipole−dipole coupling developed by Förster and the Dexter charge-transfer model, to explain the measured changes in the fluorescence properties of PQDs interacting with three different cyanine dyes using our hybrid assemblies. We first summarize the main features detailed in the Förster theory and Dexter model and then investigate the ability of those theoretical predictions to explain our experimental results.

Energy-Transfer Interaction Mechanism: Background. Within the dipole−dipole coupling formalism developed by Förster to treat fluorescence resonance energy-transfer interactions (FRET), the rate of nonradiative energy transfer between an excited donor and a ground-state proximal acceptor (one D−A pair), separated by a distance r, is expressed as[1,18]

$$k_{D-A,F} = \frac{B \times Q_D I}{\tau_D r^6} = \left(\frac{1}{\tau_D}\right) \times \left(\frac{R_0}{r}\right)^6 \tag{1a}$$

where τ_D and Q_D denote the excited-state lifetime and PL quantum yield of the donor molecule, respectively, and I is the spectral overlap integral between donor PL and acceptor absorption profiles, defined as

$$I = \int_0^\infty PL_{D-norm}(\lambda) \in_A (\lambda)\lambda^4 \, d\lambda \tag{1b}$$

The constant B is a function of the refractive index of the medium n_D, Avogadro's number N_A, and the dipole orientation factor κ_p^2:

$$B = \frac{9000(\ln 10)\kappa_p^{\,2}}{128\pi^5 n_D^{\,4} N_A} \tag{2}$$

For a configuration where the random orientation of the donor and acceptor transition dipoles is applicable to the D−A pair, a value of $\kappa_p^{\,2} = 2/3$ is used. The term R_0, in eq 1a, is the Förster radius given by

$$R_0 = (BQ_D I)^{1/6} = \left(\frac{9000(\ln 10)\kappa_p^{\,2}}{128\pi^5 n_D^{\,4} N_A} \times Q_D I\right)^{1/6} \tag{3}$$

which corresponds to a separation distance at which the energy-transfer rate is equal to the donor exciton decay rate: $k_{D-A,F}(R_0) = \frac{1}{\tau_D}$. Using the above relations, the FRET efficiency which accounts for the competition between nonradiative and radiative decay channels for the excitation energy is defined as

$$E_{ET} = \frac{k_{D-A,F}}{k_{D-A,F} + \tau_D^{\,-1}} = \frac{R_0^6}{R_0^6 + r^6} \tag{4}$$

Comparing eqs 1a and 4, one can deduce that for $r = R_0$ the energy-transfer efficiency is equal to 0.5. For a nanoscale donor (such as a spherical quantum dot made of either a conventional or an ionic perovskite semiconductor), the donor can be made to interact with equidistant surrounding acceptors. Such a configuration increases the spectral overlap integral (the ET cross-section), and the efficiency equation can then be rewritten as

$$E = \frac{\sum_i k_{D-A,i}}{\sum_i k_{D-A,i} + \tau_D^{\,-1}} = \frac{nk_{D-A,F}}{nk_{D-A,F} + \tau_D^{\,-1}} = \frac{nR_0^6}{nR_0^6 + r^6} \tag{5}$$

This implies that the presence of multiple acceptor molecules interacting with the same donor can sizably increase the ET efficiency.

In a competing and complementary energy-transfer model developed by Dexter, the interactions depend on the orbital overlap between the donor and acceptor (K) and thus require 1 to 2 nm proximity. The energy-transfer rate constant in this formalism is given by

$$k_{D-A,Dex} = Ke^{-2r/r_0} \times I' \tag{6}$$

where r_0 is the sum of the van der Waals donor and acceptor radii and I' is the normalized spectral overlap integral between the donor emission and acceptor absorption normalized spectra. The Dexter ET rate varies linearly with the overlap integral (as in the case for the Förster ET). Note that in comparison to the Förster model, the Dexter ET rate has a linear dependence on the spectral overlap I' but does not depend on the actual magnitude of the acceptor molar absorption coefficient, ε_A, or the donor fluorescence quantum yield.[1,47,48] For a configuration involving one donor interacting

https://doi.org/10.1021/acs.jpcc.5c00337
J. Phys. Chem. C 2025, 129, 4134−4145

with n proximal acceptors, one can write an expression for the ET efficiency as

$$E_{ET,Dex} = \frac{nk_{D-A,Dex}}{nk_{D-A,Dex} + \tau_D^{-1}} \quad (7)$$

The differences between the two formalisms could help distinguish whether the Förster model alone can explain our results or a combination of the two models is necessary to accurately account for the experimental data.

Experimentally, E can be determined from the steady-state fluorescence data using

$$E = 1 - \frac{F_{DA}}{F_D} \text{ (steady state)} \quad (8)$$

where the donor fluorescence intensities in the absence (F_D) or presence (F_{DA}) of the acceptor are used. Here, ET is manifested in a loss of donor fluorescence combined with sensitization of the acceptor when the latter is an emitter. Similarly, energy transfer can result in a shortening of the excited-state lifetime of the donor coupled with a lengthening of the acceptor exciton lifetime. This provides an additional means to estimate the ET efficiency of any given pair using[49]

$$E = 1 - \frac{\tau_{DA}}{\tau_D} \text{ (time-resolved)} \quad (9)$$

where τ_D and τ_{DA} respectively designate the donor excited-state lifetime in the absence and presence of the acceptors.

We hereby combine steady-state and time-resolved fluorescence spectroscopy measurements to probe the effects of varying two key parameters, namely, spectral overlap and conjugate valence. We first probe the effects of tuning the spectral overlap integral on changes in the fluorescence profiles of both the PQD donor and dye acceptor. For this, we use two representative dyes (sulfo−Cy3−Mal and sulfo−Cy5−Mal) which have cyanine conjugated architectures and solubilizing ionic groups, as shown in Figure 1A−C. The normalized emission spectra of the $CsPbBr_3$ PQD together with absorption profiles of the cyanine dyes are shown in Figure 1D. A quantum yield of 65% was measured using an integrating sphere for the $CsPbBr_3$ PQDs grown in our laboratory. The inset shows the spectral overlap function $J(\lambda)$ for each PQD−dye pair. The corresponding calculated overlap integral, I, and Förster radius, R_0, for the various PQD−dye pairs using eq 1b are provided in Table 1. Additionally, a dipole orientation factor $\kappa^2 \cong 2/3$ was used for the present hybrid, accounting for a random relative distribution of PQD and dye dipoles in the formed hybrids.[50] The use of this condition is justified for such hybrids because the coupling strategy used here relying on electrostatic interactions is expected to yield a random arrangement of the dye molecules as they self-assemble around the PQDs.[18,51]

Figure 2A,B shows the progression of the absorbance spectra and the ensemble fluorescence profiles acquired from dispersions of PQD−sulfo−Cy3 assemblies with increasing valence, n. The latter was deduced from the dye molar concentration normalized with respect to the concentration of the PQDs (fixed at 120 nM) in these experiments; the dye concentration was extracted from the absorbance data shown in Figure 2A using the molar absorption coefficient of Cy3. There is a progressive loss of PQD emission concomitant with a gradual increase in dye sensitization when n is increased. Figure 3B shows the progression of the ensemble fluorescence

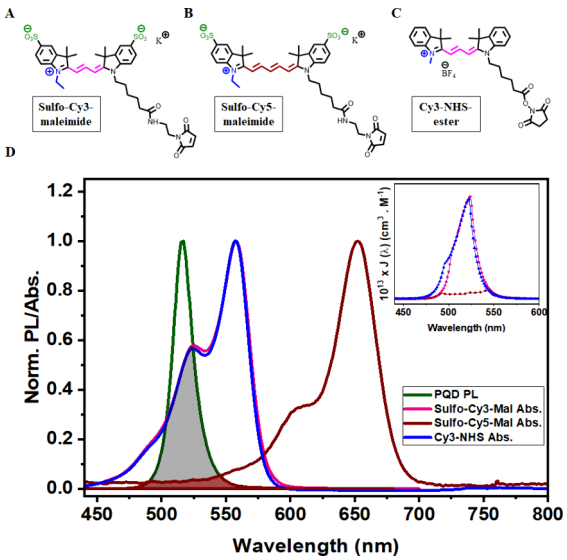

Figure 1. Chemical structures of the three distinct dyes used in this study: (A) sulfo−Cy3−Mal, (B) sulfo−Cy5−Mal, and (C) Cy3−NHS−ester. (D) Normalized UV−vis absorption spectra of the three cyanine dyes along with the PL profile of $CsPbBr_3$ PQDs. Overlap areas are highlighted in gray and brown, respectively. Plots of the spectral overlap functions, $J(\lambda)$, for PQD−sulfo−Cy3−mal, PQD−sulfo−Cy5−Mal, and PQD−Cy3−NHS−ester assemblies are shown in the inset.

spectra acquired from PQD−sulfo−Cy5 assemblies for a similar range of valences; these were extracted from the absorbance spectra in Figure 3A. The fluorescence spectra in Figure 3B show a trend similar to the one shown in Figure 2B, but the PL changes measured for the PQDs are substantially smaller. Additionally, the Cy5 sensitized emission is overall very small. We used the fluorescence data shown in Figure 2B and Figure 3B to deduce estimates for the energy-transfer efficiency, E, for both pairs at every valence n. Plots of E vs n are summarized in Figure 2C for PQD−Cy3 and in Figure 3C for PQD−Cy5. The PQD PL decay and dye sensitization increase with n are also provided. In both cases, a hyperbolic profile for E vs n is generated using the R_0 values summarized in Table 1; data can be easily fit using eq 5. We note that the efficiencies calculated from the experimental PL data (shown here and below) were carried out using the intensity at the PQD PL peak for all samples, not the integrated PL intensity.[51] Indeed, a comparison of the quenching efficiency calculated from the peak values in the composite spectra (e.g., those shown in Figure S2) to those extracted using the integrated intensity of the area under the PL peak, after deconvolution of the composite spectra for the PQD−sulfo−Cy3−Mal assemblies (e.g., those in Figure 2), yields nearly identical values. This agreement can be ascribed to the fact that the donor PL is narrow and has minimal overlap with the PL of Cy3 and Cy5.

Remark: The hyperbolic profile for E vs n is not affected by changes in [PQD]. Indeed, two additional values for E vs n collected from assemblies formed using different values ([PQD] = 60 nM and 190 nM) have been integrated into the data shown in Figure 2 without altering the hyperbolic fit to eq 5. see Figure S3.

The ensemble PL data are complemented by time-resolved fluorescence experiments. Figure 4A,B shows the PL decay profiles with time, acquired from the various PQD−Cy3 and

https://doi.org/10.1021/acs.jpcc.5c00337
J. Phys. Chem. C 2025, 129, 4134−4145

Table 1. Calculated Overlap Integral, I^a, and Förster Radius, R_0, of the Various PQD−Dye Pairs, Extracted from the Absorption and Emission Data

Donor−Acceptor Pair	Overlap Integral ($10^{13} \times I$) ($cm^3 \cdot M^{-1}$)	Förster Radius, R_0 (nm)	$10^6 \times k_{D-A,exp}$ (s^{-1})	$10^6 \times k_{D-A,theo}$ (s^{-1})
PQD−sulfo−Cy3−Mal	3.10	4.34	5.5	5.7
PQD−sulfo−Cy5−Mal	0.103	2.46	0.88	0.19
PQD-Cy3−NHS−ester	2.97	4.31	1.4	5.5

$^a I = \int_0^\infty PL_{D-norm}(\lambda)\, \epsilon_A(\lambda)\lambda^4\, d\lambda = \int_0^\infty J(\lambda)\, d\lambda$.

PQD−Cy5 assemblies used for the steady-state measurements, following a picosecond excitation with a laser pulse at 440 nm. A faster decay is measured for dispersions of conjugates with higher valences. The decay profiles were used to extract values for the average exciton lifetime, τ vs n (summarized in the Supporting Information, Table S1). The PL lifetimes were combined with eq 9 to extract estimates for ET efficiency, E. Plots of the lifetime-based efficiency vs [dye]/[PQD], summarized in Figure 4C,D, show hyperbolic profiles with efficiencies that are comparable to those generated from the steady-state data (shown in Figures 2C and 3C).

The measured changes in the PL spectra shown in Figures 2B and 3B can be attributed to nonradiative energy-transfer interactions between a central PQD (donor) and a proximal dye (Cy3 or Cy5) acceptors decorating the nanocrystal surfaces. From a first qualitative inspection, the data shown above follow the trend predicted by the Förster dipole−dipole coupling model where the smaller spectral overlap for the PQD−Cy5 pair is expected to yield smaller quenching efficiencies. However, more detailed analysis is necessary to better identify the mechanism(s) involved. For this, we first evaluate the effects of changing the spectral overlap integral, I, on the experimental ET rate, $k_{D-A,exp}$, extracted from the quenching efficiency data shown in Figures 2C and 3C (normalized to $n = 1$) using

$$k_{D-A,exp} = \frac{E_n}{n(1 - E_n)\tau_D} \tag{10}$$

Then, we compare that to the predicted/theoretical transfer rate, $k_{D-A,theo}$, extracted using eq 1a (i.e., $k_{D-A,F}$) and the overlap integral for each PQD−sulfo−Cy dye pair (see Table 1). A side-by-side comparison of the $k_{D-A,theo}$ and $k_{D-A,exp}$ values for each PQD−dye pair is provided in Table 1. We find that the experimental and theoretical rates are essentially identical for the PQD−Cy3 assemblies ($k_{D-A,exp} = 5.5 \times 10^6$ (s^{-1}) vs $k_{D-A,theo} = 5.7 \times 10^6$ (s^{-1})). However, the experimental rate is much larger than the theoretical one for the PQD−Cy5 assemblies ($k_{D-A,exp} \approx 4.63 \times k_{D-A,theo}$). These results imply that while there is good agreement between the experimental ET data and the predictions of the Förster formalism for the PQD−sulfo−Cy3 pair, the model seriously underestimates the ET rate for PQD−sulfo−Cy5. That difference may be attributed to contributions emanating from the Dexter type interactions involving charge transfer between the PQD and proximal Cy5 dye (further discussed below).[52,53] These interactions can sizably reduce the donor PL signal but would not contribute to dye sensitization. This assertion is supported by the much weaker sensitized Cy5 emission compared to the acceptor emission registered for the PQD−sulfo−Cy3 pair; compare the data in Figures 2C and 3C.

The hyperbolic profile for the E vs n plot generated from the experimental data (shown in Figures 2C and 3C) is critical as it confirms that our assemblies are made of bound PQD−dye hybrids, each with a given stoichiometry determined by the [dye]/[PQD] molar ratio used. We anticipate that binding interactions characterizing our PQDs and Cy dyes would be stronger than those expected in PQD−dye pairs explored by other groups because of the weaker ionicity of those dyes used (e.g., rhodamine B).[54] We confirm this hypothesis by applying the Benesi−Hildebrand method to determine the association constant between the quencher molecules and PQD surfaces in the solution, as recently done by Kamat's group.[41,55,56] Applying this analytical method to the fluorescence data shown in Figures 2−4 provides association constants of $K_A \approx 1.1 \times 10^8$ M^{-1} for PQD−sulfo−Cy3−Mal and 5.2×10^7 M^{-1} for PQD−sulfo−Cy5−Mal; see Supporting Information Figure S4. These values are larger by ∼2−4 orders of magnitude than those reported in the above reference, which indicates that a much stronger association combined with a slower rate of desorption is measured, in particular for the sulfo−Cy3/Cy5−Mal presenting a combined ZW moiety and a salt group. Additional details about the Benesi−Hildebrand method are provided in the Supporting Information.

Fitting the ET efficiency data for the PQD−sulfo−Cy3 assemblies to eq 5 using the Förster radius shown in Table 1 yields a value for the center-to-center distance $r \cong 7.5$ nm (for a spherical symmetry). That value is reasonable if we consider a few characteristic facts about the nanocrystals. We approximate the dye by a sphere with radius 0.6 nm. The cubic morphology of the PQD affects the distribution of r for dyes at/near the center of the facets differently, compared to those near the edges and corners of the cube. Dyes located near the center of the facets have the shortest distance $r \approx 4.7$ nm (4.1 + 0.6 nm), which encompasses a small fraction of the total number of dyes per PQD−dye assembly. Conversely, acceptors distributed in areas near the corners and edges of the cube have longer separation distances, ∼7.7 nm for corners and ∼6.5 nm for edges. There are 6 facets, 8 corners, and 12 edges in each PQD cube. This implies that the larger fraction of attached dyes is located in areas farther from the center. An inspection of the TEM image shown in Figure 5 for a single nanocrystal indicates that the cube's corners are not sharp, making the PQD appear like a smooth cuboid and the separation distance near the corners slightly smaller (∼7.5 nm). Combining these observations with heterogeneities in nanocrystal size and dye orientation on the PQD surfaces would imply that an average center-to-center distance for dyes distributed around the PQD surface of 7.5 nm is reasonable for our assemblies. This agreement further supports the above results that the dipole−dipole coupling formalism characterizes the ET interactions well for the PQD−sulfo−Cy3 pair.

Next, we used photoluminescence excitation (PLE) spectroscopy to identify the main absorbing species in the assemblies that contribute to the measured dye emission. We focused on the dispersions of PQD−sulfo−Cy3 and PQD−sulfo−Cy5. For this, we tracked the dye emission integrated over a narrow range at the PL peak (580 nm) while scanning the excitation signal from 350 to 800 nm for PQD−sulfo−Cy3.

https://doi.org/10.1021/acs.jpcc.5c00337
J. Phys. Chem. C 2025, 129, 4134−4145

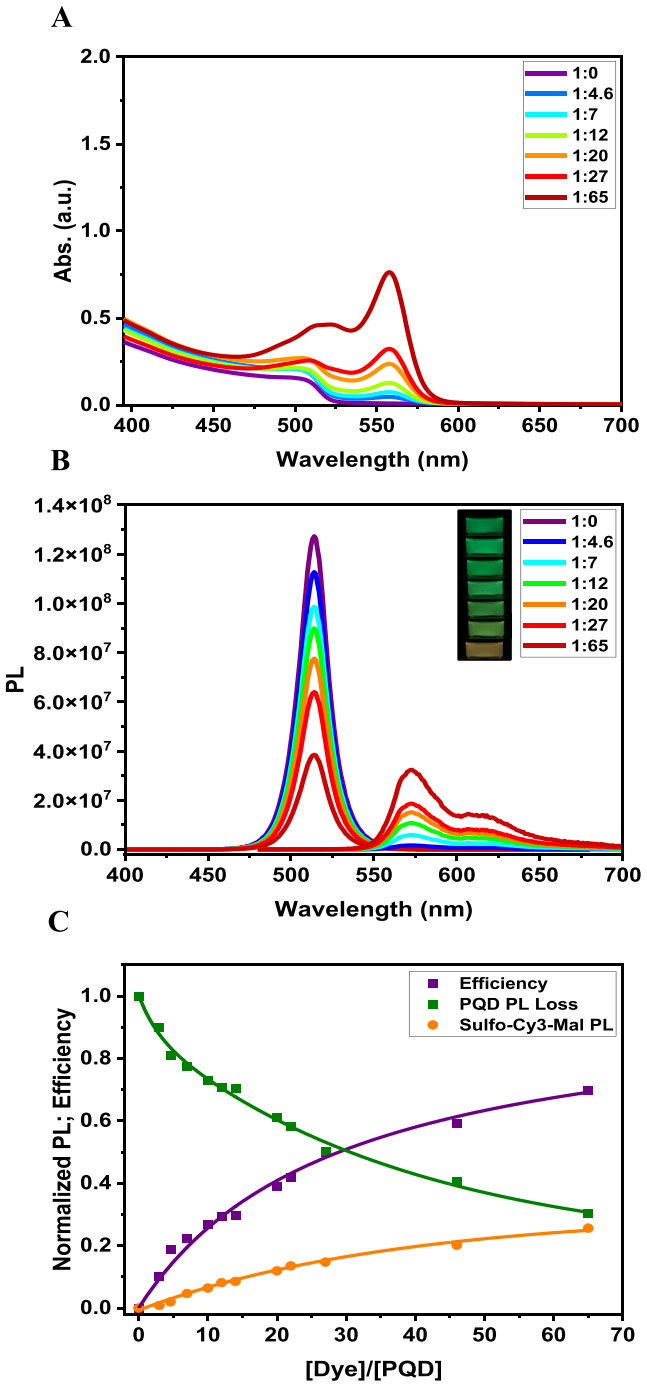

Figure 2. (A) Select sets of UV−vis absorption and (B) deconvoluted PL spectra measured from the PQD−sulfo−Cy3 assemblies formed with an increasing [dye]/[PQD] ratio. Samples were excited at 365 nm. The contribution from direct dye excitation was subtracted from each spectrum. Only selected profiles are shown; the full set of data can be found in Figure S1. (C) Plots of the relative PQD PL loss (green squares), FRET efficiency vs valence (purple squares), and dye PL normalized with respect to that of PQDs (orange spheres). The efficiency data were fit to eq 5 by using the R_0 values in Table 1.

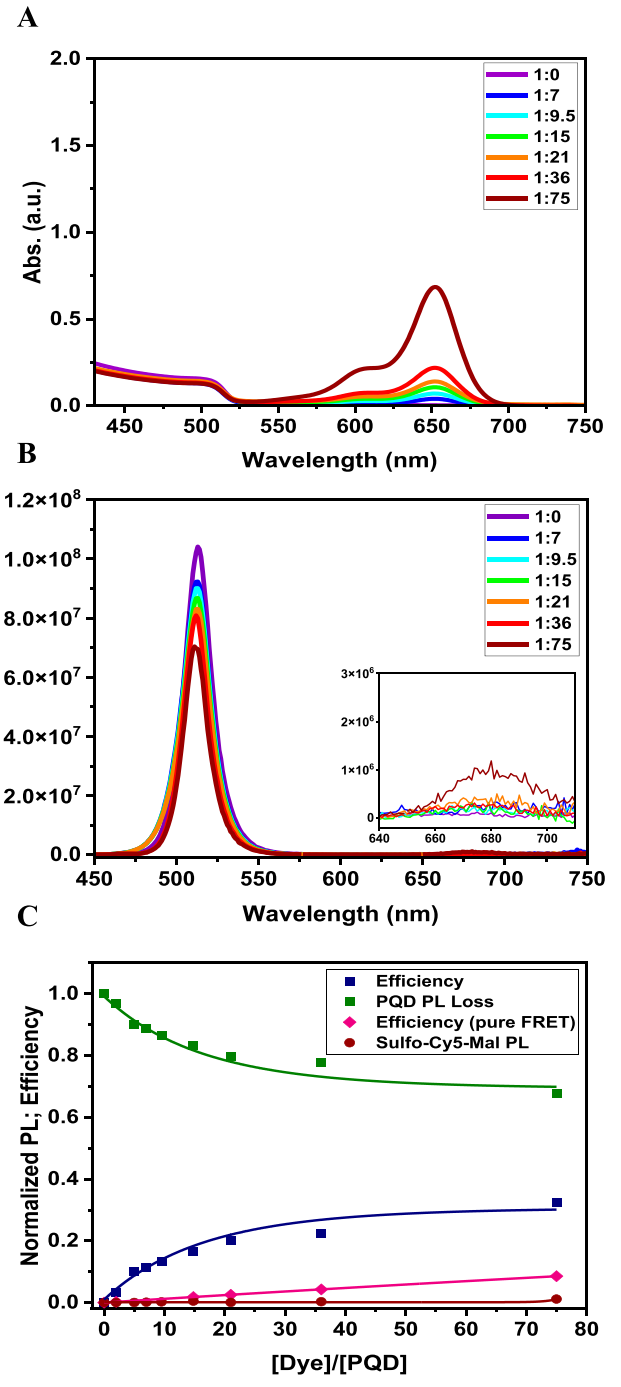

Figure 3. (A) UV−vis absorption and (B) PL spectra acquired from the PQD−sulfo−Cy5 assemblies with an increasing [dye]/[PQD] ratio. (C) Plots of the relative PQD PL loss (green squares), ET efficiency vs valence (blue squares), predicted efficiency based on the Förster model (magenta diamonds), and normalized dye PL (maroon spheres). The efficiency data were fit to a hyperbolic function shown in eq 5, as done in Figure 2.

A similar protocol was applied to the PQD−sulfo−Cy5 sample, but the dye emission was collected at the Cy5 peak (680 nm). The PLE spectra shown in Figure 6A,B, indicate that the dye sensitization for both pairs is primarily triggered by excitation of the central PQD up to the band edge wavelength (at ∼507 nm). In comparison, the signal generated using excitation beyond the PQD absorption band edge emanates exclusively from direct excitation of the dye in the assemblies. Additionally, the spectra shown in Figure 6A,B can be deconvoluted into a PQD absorption profile and dye absorption. This confirms the formation of a singlet excited dye as a result of resonant energy transfer from $CsPbBr_3$ PQDs. Finally, we should note that the PLE spectra after deconvolution show that the dye signal promoted by excitation

https://doi.org/10.1021/acs.jpcc.5c00337
J. Phys. Chem. C 2025, 129, 4134−4145

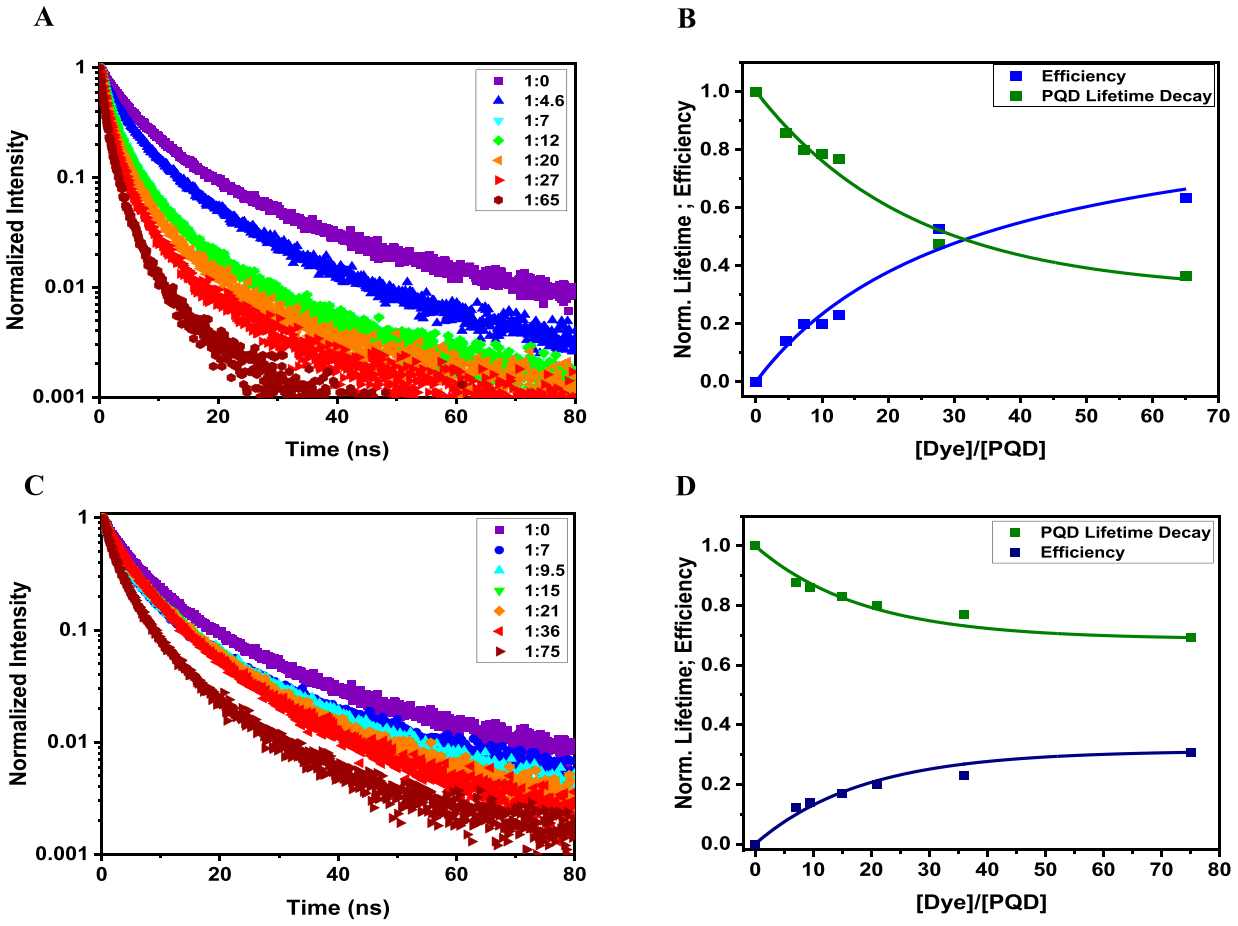

Figure 4. PL lifetime decay profiles acquired from (A) PQD−sulfo−Cy3 and (B) PQD−sulfo−Cy5 assemblies. Data for several [dye]/[PQD] ratios are shown. Plot of the normalized PQD fluorescence lifetime side-by-side with the corresponding efficiency data for (C) PQD−sulfo−Cy3 and for (D) PQD−sulfo−Cy5 assemblies.

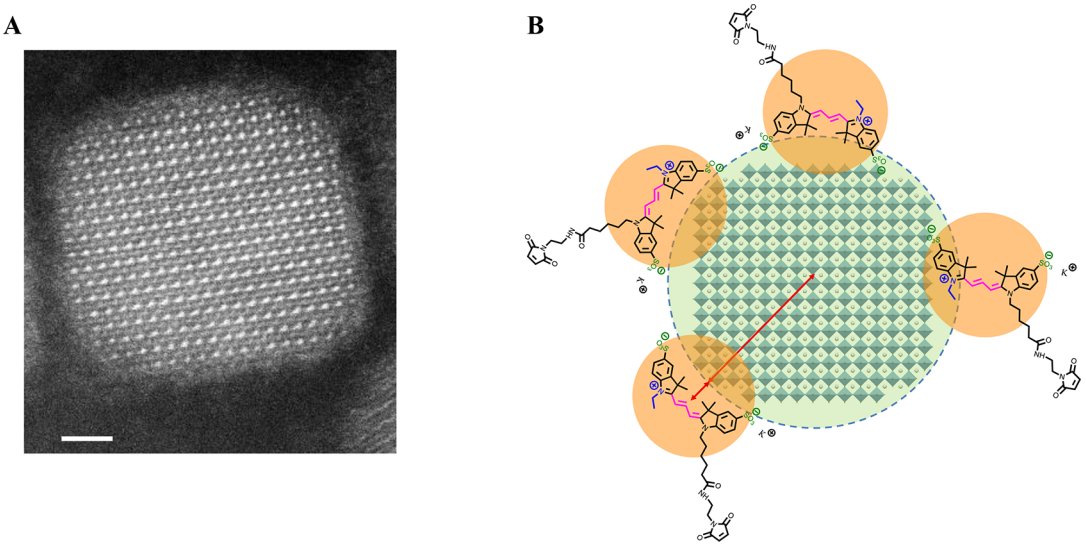

Figure 5. (A) HRSTEM image of an individual PQD with resolved crystal planes. (B) Schematic representation of the estimation of the PQD−dye distance using the equivalent sphere extracted from the average edge length of the $CsPbBr_3$ cube with sulfo−Cy3 dye.

of the PQDs is much larger for the PQD−Cy3 pair than for the PQD−Cy5 pair; see Figure 6A,B. This clearly reflects the higher rate of resonance nonradiative energy transfer from PQD to Cy3 acceptors compared to Cy5. It is consistent with the results shown in Figures 2 and 3 and the ensuing discussion above.

Finally, we tested the configuration where the PQDs are mixed with Cy3−NHS ester, which presents only one ammonium salt in its structure. Thus, interactions with the

https://doi.org/10.1021/acs.jpcc.5c00337
J. Phys. Chem. C 2025, 129, 4134−4145

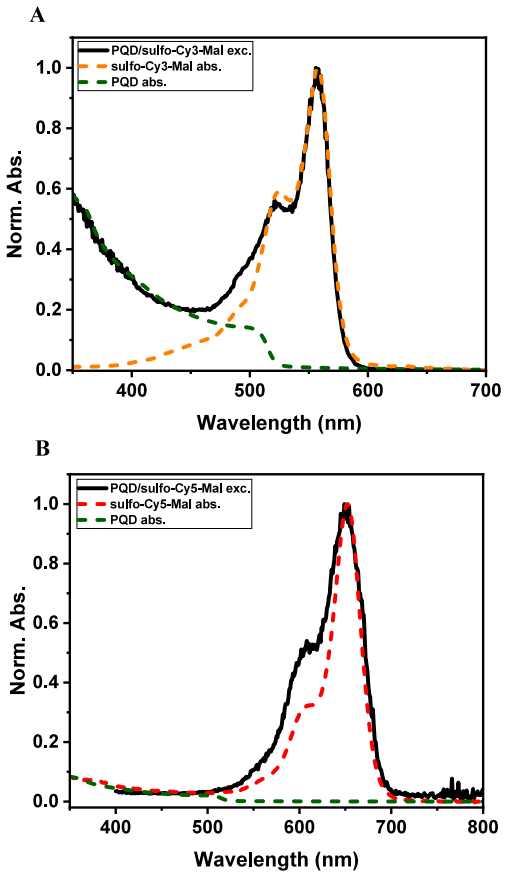

Figure 6. (A) Photoluminescence excitation spectrum of the PQD−sulfo−Cy3−Mal assembly together with the absorption profiles of PQD only and dye only. (B) Photoluminescence excitation spectrum of the PQD−sulfo−Cy5−Mal assembly together with the absorption profiles of PQD only and dye only. We used [Cy3]:[PQD] = 65:1 and [Cy5]:[PQD] = 75:1 for these measurements.

nanocrystal surfaces, attributed to complexation with the ammonium groups, are expected to be weaker than those governing PQD−sulfo−Cy3/Cy5 systems. Estimates of the [dye]/[PQD] ratio in the dispersions were deduced from the absorption spectra measured for the PQD-plus-dye mixture, as above. Figure 7A shows the fluorescent profiles acquired from dispersions with an increasing dye-to-PQD ratio. There is a progressive loss of nanocrystal fluorescence coupled with an increase in dye emission similar to what is shown for PQD−sulfo−Cy3 in Figure 2. However, the plot of the efficiency vs [dye]/[PQD] molar ratio is not hyperbolic. Instead, the measured efficiency data exhibit a linear dependence on [dye]/[PQD] (Figure 7B), which is more indicative of collisional quenching. Figure S5 shows a linear fit of the data using Stern−Volmer analysis for the PQD−Cy3−NHS−ester assemblies. The ensemble PL data are further supported by time-resolved fluorescence decay profiles from PQD−Cy3−NHS−ester dispersions; see Figure 7C,D. The efficiency results extracted from the steady-state and lifetime data are essentially identical. Application of the Benesi−Hildebrand analysis has yielded $K_A \approx 5 \times 10^6$ M^{-1} for this pair, ∼2 orders of magnitude smaller than the one measured for the PQD−sulfo−Cy3−Mal pair (see Table 2). Additionally, we note that the ET rate, $k_{D-A,exp}$, is ∼4 times smaller than the one measured for PQD−sulfo−Cy3−Mal.

We now discuss our experimental results within the framework of the Förster dipole−dipole coupling and the Dexter electron-transfer formalisms. We also compare our findings to those of recent literature reports. Our combined results suggest that a process consistent with a resonant dipole−dipole interaction model provides a good interpretation for the data acquired for the Br-based PQD−sulfo−Cy3 system, where the measured ET rate is essentially identical to that predicted by the model. For these assemblies, spectral overlap, spatial proximity, and conjugate stoichiometry play roles in controlling the ET process and its efficiency, as shown in Figure 2. However, we found that even though the total ET efficiency measured for PQD−sulfo−Cy5 was much smaller than the efficiency measured for PQD−sulfo−Cy3, the PL quenching registered for this pair sizably exceeds the value predicted by the Förster dipole coupling model (Figure 3). This indicates that there is an additional nonradiative pathway for donor excitation decay which requires close proximity to the nanocrystal, namely Dexter type, where ET efficiency strongly depends on the orbital overlap between donor and acceptor.

Overall, the above results complement the findings reported by Davis and co-workers, Kamat and co-workers, and more recently Kovalenko and co-workers.[40−42,54,57−59] For instance, Kovalenko and co-workers used single-molecule experiments to probe the proximity interaction between $CsPbBr_3$ PQD and Cy3-NHS and measured ET rates that are consistent with the Förster formalism.[42] Kamat's group used blue-emitting $CsPb(Cl/Br)_3$ or green-emitting $CsPbBr_3$ donors and rhodamine-based acceptors. They reported ET rates that support the Förster model for $CsPbBr_3$−RhB mixtures with increasing [dye]/[PQD].[41] However, they found that when using mixed halide donors with varying Cl/Br molar fractions to generate blue PL and vary the spectral overlap with RhB, the measured ET transfer rates sizably exceeded the prediction of the Förster model. They attributed the difference to a Dexter charge-transfer process favored by better coupling K.[52] The main difference between our configuration and theirs is the reagent concentrations used; our [dye]/[PQD] ratio varied over the range of ∼2.5−120, while theirs were 1 order of magnitude larger, approximately ∼33−840. Our study probed the effects of tuning the spectral overlap using sulfo−Cy3−Mal and sulfo−Cy5−Mal as well as the binding affinity of dye acceptors by comparing hybrids assembled using sulfo−Cy3−Mal and sulfo−Cy3−NHS−ester, which exhibit drastically different affinities for $CsPbBr_3$ cores, as indicated by the Benesi−Hildebrand analysis. Our PQDs have been ligand substituted with a higher coordination polyzwitterion coating. Due to their small size and the strong affinity of the zwitterion motifs for the PQD surfaces, the sulfo dyes diffuse through the coating and interact with the inorganic cores. In a recent study, Ginger and co-workers combined single-molecule blinking experiments with first-principles calculations to show that at equilibrium molecular zwitterion lecithin exhibits much stronger binding energy on $CsPbBr_3$ QDs than the native oleic acid/oleylamine coating, which agrees with our rationale.[60] The ET efficiencies extracted from steady-state and time-resolved PL exhibit a hyperbolic profile for the E versus [Cy3/Cy5−Mal]/[PQD] ratio, confirming stable PQD−dye association. However, when NHS−ester-modified Cy3 dyes are used, the ET data suggest a rather collisional interaction process, where a linear dependence on the valence is observed, confirming that weaker interactions characterize this D−A pair.

https://doi.org/10.1021/acs.jpcc.5c00337
J. Phys. Chem. C 2025, 129, 4134−4145

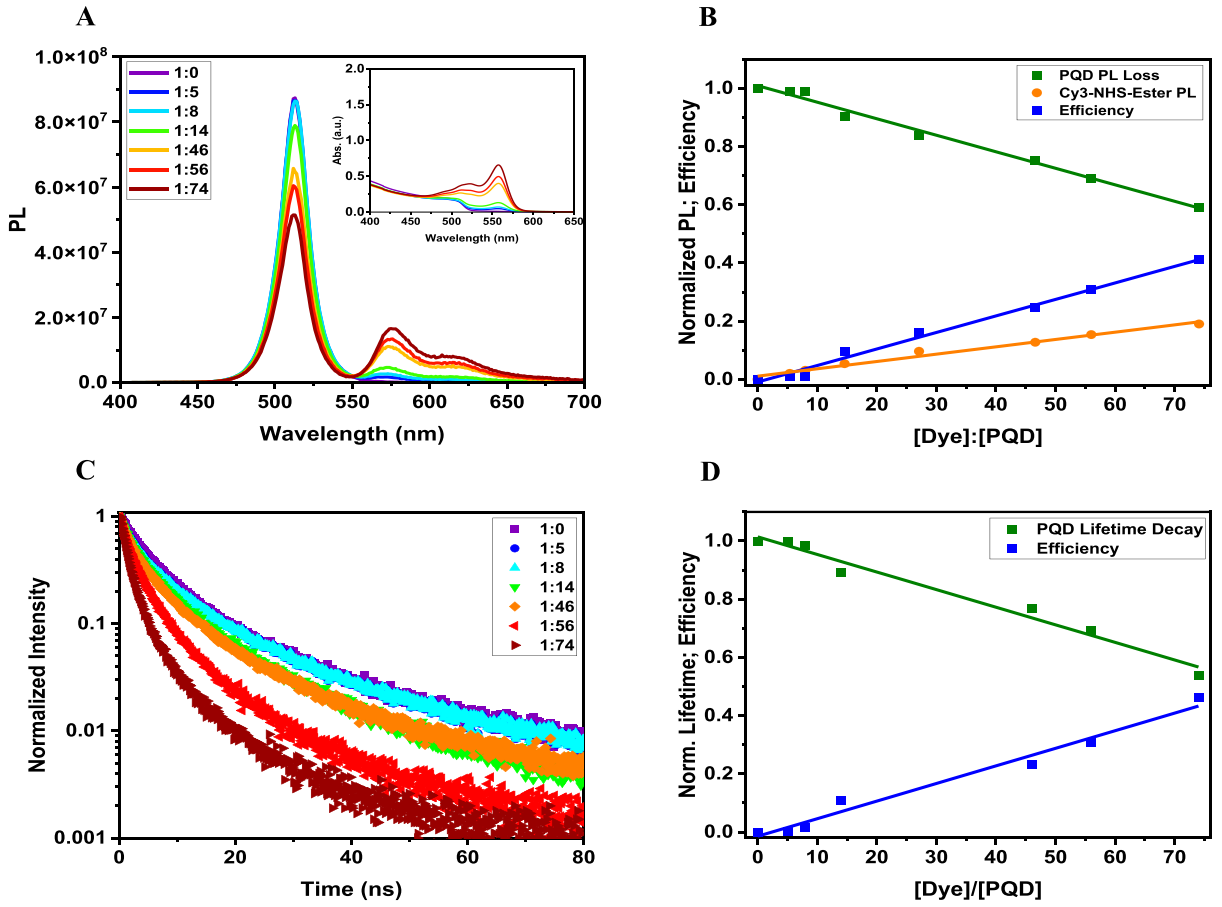

Figure 7. (A) PL spectra of the PQD−Cy3−NHS−ester assemblies formed with varying [dye]/[PQD] ratios. The UV−vis absorption spectra are shown as an inset. (B) Plots of the relative PQD PL decay (green squares), enhanced dye emission normalized with respect to the PQD signal (orange spheres), and corresponding efficiency data (blue squares). The efficiency data show a more linear trend, not a hyperbolic profile. This is attributed to a lack of stable Cy3−NHS−ester binding for these assemblies. (C) PL lifetime profiles measured for the PQD−Cy3−NHS−ester assemblies. (D) Plots of the normalized lifetime decay along with the corresponding efficiency values.

Table 2. Values for the Association Constants, K_A, Extracted from the Fluorescence Data Analysis Using the Benesi−Hildebrand Method

D−A pair	K_A (M^{-1})
PQD−Cy3−sulfo−Mal	1.1×10^8
PQD−Cy5−sulfo−Mal	5.2×10^7
PQD−Cy3−NHS ester	5×10^6

We should add that a mix of Förster and non-Förster ET quenching has been reported for CdSe−ZnS QD−dye pairs depending on the spectral overlap integrals.[18,23,50,51,61] In particular, larger non-Förster-induced PL quenching of CdSe−ZnS QDs, chemically coupled to Cy5 and Cy7 dye acceptors, has been reported by Zamkov and coworkers. A much weaker Förster contribution to the total energy transfer was measured for Cy7 compared to that of QD−Cy5 pairs.[22]

CONCLUSIONS

We have characterized the energy-transfer interactions in hybrid PQD−dye donor−acceptor assemblies. We employed $CsPbBr_3$ nanocrystals and various cyanine dye molecules that present zwitterionic moieties and salt groups to promote conjugation between PQD and dyes via electrostatic binding while tuning the spectral overlap and binding affinity. By controlling the donor−acceptor proximity and varying the spectral overlap through the structures of cyanine dyes, we formed a unique system suitable for investigating energy-transfer interactions in PQD−dye assemblies. Combining steady-state and time-resolved fluorescence experiments, we measured strong ET interactions, with efficiencies that depend on a few key parameters outlined in the Förster dipole−dipole coupling model, namely, spectral overlap, spatial proximity, and valence promoted by stable binding and the number of dyes interacting with an individual PQD in each assembly. However, quantitatively accounting for the measured PL changes is better achieved by invoking a combination of the Förster dipole−dipole coupling and the Dexter electron-transfer mechanisms, in particular, for the pair with the weaker spectral overlap. Our investigation not only advances our understanding of ET mechanisms applied to PQD−dye systems but also underscores the potential of such systems for applications in energy harvesting and sensing. Our approach could be easily expanded to probe ET interactions involving other colloidal PQDs with different sizes, shapes, compositions, and stabilizing surface ligands. Additional characterization relying on transient absorption measurements using PQDs assembled with sulfo dyes that exhibit varying degrees of spectral overlap is underway, which would provide additional and valuable insights into the ET interactions in such donor−acceptor pairs.

https://doi.org/10.1021/acs.jpcc.5c00337
J. Phys. Chem. C 2025, 129, 4134−4145

■ ASSOCIATED CONTENT

Supporting Information

The Supporting Information is available free of charge at https://pubs.acs.org/doi/10.1021/acs.jpcc.5c00337.

Additional information on polymer ligand synthesis, instrumentation, TEM data, and time-resolved PL (PDF)

■ AUTHOR INFORMATION

Corresponding Author

Hedi Mattoussi − *Department of Chemistry and Biochemistry, Florida State University, Tallahassee, Florida 32306, United States;* orcid.org/0000-0002-6511-9323; Email: mattoussi@chem.fsu.edu

Authors

Selin E. Donmez − *Department of Chemistry and Biochemistry, Florida State University, Tallahassee, Florida 32306, United States;* Present Address: National Center for Toxicological Research, U.S. Food and Drug Administration, Jefferson, AR 72079, United States; orcid.org/0000-0002-1377-2689

Sisi Wang − *Department of Chemistry and Biochemistry, Florida State University, Tallahassee, Florida 32306, United States;* Present Address: ASM America, Inc., Phoenix, AZ 85034, United States

Unaisah Vorajee − *Department of Chemistry and Biochemistry, Florida State University, Tallahassee, Florida 32306, United States*

Geoffrey F. Strouse − *Department of Chemistry and Biochemistry, Florida State University, Tallahassee, Florida 32306, United States;* orcid.org/0000-0003-0841-282X

Complete contact information is available at: https://pubs.acs.org/10.1021/acs.jpcc.5c00337

Notes

The authors declare no competing financial interest.

■ ACKNOWLEDGMENTS

We thank FSU and the National Science Foundation (NSF-CHE, grant no. 2005079), AFOSR (grant no. FA9550-18-1-0144), the National Institutes of Health (RO1DK133464), and Kasei-Asahi Corporation for financial support. This research used resources provided by the X-ray Crystallography Center at the FSU Department of Chemistry and Biochemistry (FSU075000XRAY). The TEM images were acquired at the National High Magnetic Field Laboratory, which is supported by National Science Foundation Cooperative Agreement No. DMR-1644779 and the State of Florida.

■ REFERENCES

(1) Lakowicz, J. R. *Principles of Fluorescence Spectroscopy*, 3rd ed.; Springer: New York, 2006.

(2) Roy, R.; Hohng, S.; Ha, T. A practical guide to single-molecule FRET. *Nat. Methods* **2008**, *5*, 507−516.

(3) Miyawaki, A. Visualization of the spatial and temporal dynamics of intracellular signaling. *Dev. Cell* **2003**, *4*, 295−305.

(4) Jares-Erijman, E. A.; Jovin, T. M. FRET imaging. *Nat. Biotechnol.* **2003**, *21*, 1387−1395.

(5) Lerner, E.; Cordes, T.; Ingargiola, A.; Alhadid, Y.; Chung, S.; Michalet, X.; Weiss, S. Toward dynamic structural biology: Two decades of single-molecule Förster resonance energy transfer. *Science* **2018**, *359* (6373), eaan1133.

(6) Lerner, E.; Barth, A.; Hendrix, J.; Ambrose, B.; Birkedal, V.; Blanchard, S. C.; Börner, R.; Sung Chung, H.; Cordes, T.; Craggs, T. D.; et al. FRET-based dynamic structural biology: Challenges, perspectives and an appeal for open-science practices. *eLife* **2021**, *10*, No. e60416.

(7) Sapsford, K. E.; Berti, L.; Medintz, I. L. Materials for Fluorescence Resonance Energy Transfer Analysis: Beyond Traditional Donor-Acceptor Combinations. *Angew. Chem., Int. Ed.* **2006**, *45*, 4562−4589.

(8) Murray, C. B.; Norris, D. J.; Bawendi, M. G. Synthesis and characterization of nearly monodisperse CdE (E = S, Se, Te) semiconductor nanocrystallites. *J. Am. Chem. Soc.* **1993**, *115*, 8706−8715.

(9) Bruchez, M.; Moronne, M.; Gin, P.; Weiss, S.; Alivisatos, A. P. Semiconductor nanocrystals as fluorescent biological labels. *Science* **1998**, *281* (5385), 2013−2016.

(10) Mattoussi, H.; Mauro, J. M.; Goldman, E. R.; Anderson, G. P.; Sundar, V. C.; Mikulec, F. V.; Bawendi, M. G. Self-assembly of CdSe-ZnS quantum dot bioconjugates using an engineered recombinant protein. *J. Am. Chem. Soc.* **2000**, *122*, 12142−12150.

(11) Medintz, I. L.; Clapp, A. R.; Mattoussi, H.; Goldman, E. R.; Fisher, B.; Mauro, J. M. Self-assembled nanoscale biosensors based on quantum dot FRET donors. *Nat. Mater.* **2003**, *2*, 630−638.

(12) Alivisatos, P. The use of nanocrystals in biological detection. *Nat. Biotechnol.* **2004**, *22*, 47−52.

(13) Michalet, X.; Pinaud, F.; Bentolila, L.; Tsay, J.; Doose, S.; Li, J.; Sundaresan, G.; Wu, A.; Gambhir, S.; Weiss, S. Quantum dots for live cells, in vivo imaging, and diagnostics. *Science* **2005**, *307*, 538−544.

(14) Medintz, I.; Uyeda, H.; Goldman, E.; Mattoussi, H. Quantum dot bioconjugates for imaging, labelling and sensing. *Nat. Mater.* **2005**, *4*, 435−446.

(15) Clapp, A. R.; Medintz, I. L.; Mattoussi, H. Förster Resonance Energy Transfer Investigations Using Quantum-Dot Fluorophores. *ChemPhysChem* **2006**, *7*, 47−57.

(16) Klostranec, J. M.; Chan, W. C. W. Quantum Dots in Biological and Biomedical Research: Recent Progress and Present Challenges. *Adv. Mater.* **2006**, *18*, 1953−1964.

(17) Mattoussi, H.; Palui, G.; Na, H. B. Luminescent quantum dots as platforms for probing in vitro and in vivo biological processes. *Adv. Drug. Deliver. Rev.* **2012**, *64*, 138−166.

(18) Medintz, I. L.; Mattoussi, H. Quantum dot-based resonance energy transfer and its growing application in biology. *Phys. Chem. Chem. Phys.* **2009**, *11*, 17−45.

(19) Hildebrandt, N.; Spillmann, C. M.; Algar, W. R.; Pons, T.; Stewart, M. H.; Oh, E.; Susumu, K.; Díaz, S. A.; Delehanty, J. B.; Medintz, I. L. Energy Transfer with Semiconductor Quantum Dot Bioconjugates: A Versatile Platform for Biosensing, Energy Harvesting, and Other Developing Applications. *Chem. Rev.* **2017**, *117*, 536−711.

(20) Kagan, C. R.; Murray, C. B.; Nirmal, M.; Bawendi, M. G. Electronic energy transfer in CdSe quantum dot solids. *Phys. Rev. Lett.* **1996**, *76*, 3043−3043.

(21) Kagan, C. R.; Murray, C. B.; Bawendi, M. G. Long-range resonance transfer of electronic excitations in close-packed CdSe quantum-dot solids. *Phys. Rev. B* **1996**, *54*, 8633−8643.

(22) Moroz, P.; Jin, Z.; Sugiyama, Y.; Lara, D. A.; Razgoniaeva, N.; Yang, M.; Kholmicheva, N.; Khon, D.; Mattoussi, H.; Zamkov, M. Competition of Charge and Energy Transfer Processes in Donor-Acceptor Fluorescence Pairs: Calibrating the Spectroscopic Ruler. *ACS Nano* **2018**, *12*, 5657−5665.

(23) Xia, C.; Wang, W.; Du, L.; Rabouw, F. T.; van den Heuvel, D. J.; Gerritsen, H. C.; Mattoussi, H.; de Mello Donega, C. Förster Resonance Energy Transfer between Colloidal CuInS2/ZnS Quantum Dots and Dark Quenchers. *J. Phys.Chem. C* **2020**, *124*, 1717−1731.

(24) Roy, P.; Devatha, G.; Roy, S.; Rao, A.; Pillai, P. P. Electrostatically Driven Resonance Energy Transfer in an All-Quantum Dot Based Donor-Acceptor System. *J. Phys. Chem. Lett.* **2020**, *11*, 5354−5360.

(25) Rajan, D.; Muraleedharan, A.; Variyar, A.; Verma, P.; Pinhero, F.; Lakshmanna, Y. A.; Sabari Sankar, T.; Thomas, K. G. Single- and two-photon-induced Förster resonance energy transfer in InP-mCherry bioconjugates. *J. Chem. Phys.* **2024**, *160*, 044712.
(26) Thirunavukkuarasu, S.; George, A.; Thomas, A.; Thomas, A.; Vijayan, V.; Thomas, K. G. InP Quantum Dots: Probing the Active Domain of Tau Peptide Using Energy Transfer. *J. Phys. Chem. C* **2018**, *122*, 14168−14176.
(27) Thomas, A.; Nair, P. V.; George Thomas, K. InP Quantum Dots: An Environmentally Friendly Material with Resonance Energy Transfer Requisites. *J. Phys. Chem. C* **2014**, *118*, 3838−3845.
(28) Charbonnière, L. J.; Hildebrandt, N.; Ziessel, R. F.; Löhmannsröben, H.-G. Lanthanides to Quantum Dots Resonance Energy Transfer in Time-Resolved Fluoro-Immunoassays and Luminescence Microscopy. *J. Am. Chem. Soc.* **2006**, *128*, 12800−12809.
(29) Algar, W. R.; Wegner, D.; Huston, A. L.; Blanco-Canosa, J. B.; Stewart, M. H.; Armstrong, A.; Dawson, P. E.; Hildebrandt, N.; Medintz, I. L. Quantum Dots as Simultaneous Acceptors and Donors in Time-Gated Förster Resonance Energy Transfer Relays: Characterization and Biosensing. *J. Am. Chem. Soc.* **2012**, *134*, 1876−1891.
(30) Clapp, A. R.; Medintz, I. L.; Fisher, B. R.; Anderson, G. P.; Mattoussi, H. Can Luminescent Quantum Dots Be Efficient Energy Acceptors with Organic Dye Donors? *J. Am. Chem. Soc.* **2005**, *127*, 1242−1250.
(31) Ast, S.; Rutledge, P. J.; Todd, M. H. The properties and performance of a pH-responsive functionalised nanoparticle. *Faraday Discuss.* **2014**, *175*, 171−187.
(32) Ast, S.; Rutledge, P. J.; Todd, M. H. pH-Responsive quantum dots (RQDs) that combine a fluorescent nanoparticle with a pH-sensitive dye. *Phys. Chem. Chem. Phys.* **2014**, *16*, 25255−25257.
(33) Tsai, H.; Nie, W.; Blancon, J.-C.; Stoumpos, C. C.; Asadpour, R.; Harutyunyan, B.; Neukirch, A. J.; Verduzco, R.; Crochet, J. J.; Tretiak, S.; et al. High-efficiency two-dimensional Ruddlesden-Popper perovskite solar cells. *Nature* **2016**, *536*, 312.
(34) Xing, G.; Mathews, N.; Lim, S. S.; Yantara, N.; Liu, X.; Sabba, D.; Grätzel, M.; Mhaisalkar, S.; Sum, T. C. Low-temperature solution-processed wavelength-tunable perovskites for lasing. *Nat. Mater.* **2014**, *13*, 476.
(35) Huang, H.; Bodnarchuk, M. I.; Kershaw, S. V.; Kovalenko, M. V.; Rogach, A. L. Lead Halide Perovskite Nanocrystals in the Research Spotlight: Stability and Defect Tolerance. *ACS Energy Lett.* **2017**, *2*, 2071−2083.
(36) Zhou, H.; Chen, Q.; Li, G.; Luo, S.; Song, T.-b.; Duan, H.-S.; Hong, Z.; You, J.; Liu, Y.; Yang, Y. Interface engineering of highly efficient perovskite solar cells. *Science* **2014**, *345* (6196), 542−546.
(37) Grätzel, M. The light and shade of perovskite solar cells. *Nat. Mater.* **2014**, *13*, 838−842.
(38) Tian, Y.; Zhou, C.; Worku, M.; Wang, X.; Ling, Y.; Gao, H.; Zhou, Y.; Miao, Y.; Guan, J.; Ma, B. Highly Efficient Spectrally Stable Red Perovskite Light-Emitting Diodes. *Adv. Mater.* **2018**, *30*, 1707093.
(39) Pan, J.; Quan, L. N.; Zhao, Y.; Peng, W.; Murali, B.; Sarmah, S. P.; Yuan, M.; Sinatra, L.; Alyami, N. M.; Liu, J.; et al. Highly Efficient Perovskite-Quantum-Dot Light-Emitting Diodes by Surface Engineering. *Adv. Mater.* **2016**, *28*, 8718−8725.
(40) Rossi, A.; Price, M. B.; Hardy, J.; Gorman, J.; Schmidt, T. W.; Davis, N. J. L. K. Energy Transfer between Perylene Diimide Based Ligands and Cesium Lead Bromide Perovskite Nanocrystals. *J. Phys. Chem. C* **2020**, *124*, 3306−3313.
(41) DuBose, J. T.; Kamat, P. V. Directing Energy Transfer in Halide Perovskite-Chromophore Hybrid Assemblies. *J. Am. Chem. Soc.* **2021**, *143*, 19214−19223.
(42) Feld, L. G.; Boehme, S. C.; Morad, V.; Sahin, Y.; Kaul, C. J.; Dirin, D. N.; Rainò, G.; Kovalenko, M. V. Quantifying Förster Resonance Energy Transfer from Single Perovskite Quantum Dots to Organic Dyes. *ACS Nano* **2024**, *18*, 9997−10007.
(43) Protesescu, L.; Yakunin, S.; Bodnarchuk, M. I.; Krieg, F.; Caputo, R.; Hendon, C. H.; Yang, R. X.; Walsh, A.; Kovalenko, M. V. Nanocrystals of Cesium Lead Halide Perovskites (CsPbX3, X = Cl, Br, and I): Novel Optoelectronic Materials Showing Bright Emission with Wide Color Gamut. *Nano Lett.* **2015**, *15*, 3692−3696.
(44) Wang, S.; Du, L.; Donmez, S.; Xin, Y.; Mattoussi, H. Polysalt ligands achieve higher quantum yield and improved colloidal stability for CsPbBr3 quantum dots. *Nanoscale* **2021**, *13*, 16705−16718.
(45) Wang, S.; Du, L.; Jin, Z.; Xin, Y.; Mattoussi, H. Enhanced Stabilization and Easy Phase Transfer of CsPbBr3 Perovskite Quantum Dots Promoted by High-Affinity Polyzwitterionic Ligands. *J. Am. Chem. Soc.* **2020**, *142*, 12669−12680.
(46) De Roo, J.; Ibáñez, M.; Geiregat, P.; Nedelcu, G.; Walravens, W.; Maes, J.; Martins, J. C.; Van Driessche, I.; Kovalenko, M. V.; Hens, Z. Highly Dynamic Ligand Binding and Light Absorption Coefficient of Cesium Lead Bromide Perovskite Nanocrystals. *ACS Nano* **2016**, *10*, 2071−2081.
(47) Dexter, D. L. A Theory of Sensitized Luminescence in Solids. *J. Chem. Phys.* **1953**, *21*, 836−850.
(48) Zheng, K.; Žídek, K.; Abdellah, M.; Zhu, N.; Chábera, P.; Lenngren, N.; Chi, Q.; Pullerits, T. Directed Energy Transfer in Films of CdSe Quantum Dots: Beyond the Point Dipole Approximation. *J. Am. Chem. Soc.* **2014**, *136*, 6259−6268.
(49) Gopich, I. V.; Szabo, A. Theory of the energy transfer efficiency and fluorescence lifetime distribution in single-molecule FRET. *Proc. Natl. Acad. Sci. U.S.A.* **2012**, *109*, 7747−7752.
(50) Medintz, I. L.; Pons, T.; Susumu, K.; Boeneman, K.; Dennis, A. M.; Farrell, D.; Deschamps, J. R.; Melinger, J. S.; Bao, G.; Mattoussi, H. Resonance Energy Transfer Between Luminescent Quantum Dots and Diverse Fluorescent Protein Acceptors. *J. Phys. Chem. C* **2009**, *113*, 18552−18561.
(51) Clapp, A. R.; Medintz, I. L.; Mauro, J. M.; Fisher, B. R.; Bawendi, M. G.; Mattoussi, H. Fluorescence resonance energy transfer between quantum dot donors and dye-labeled protein acceptors. *J. Am. Chem. Soc.* **2004**, *126*, 301−310.
(52) Wang, C.; Malinoski, A.; Yuan, J.; Brea, C.; Hu, G. A Surface Engineering Approach for Promoting Dexter Energy Transfer from Lead Halide Perovskite Nanocrystals. *J. Phys. Chem. C* **2023**, *127*, 1135−1144.
(53) Wu, K.; Liang, G.; Shang, Q.; Ren, Y.; Kong, D.; Lian, T. Ultrafast Interfacial Electron and Hole Transfer from CsPbBr3 Perovskite Quantum Dots. *J. Am. Chem. Soc.* **2015**, *137*, 12792−12795.
(54) DuBose, J. T.; Kamat, P. V. How Pendant Groups Dictate Energy and Electron Transfer in Perovskite-Rhodamine Light Harvesting Assemblies. *J. Am. Chem. Soc.* **2023**, *145*, 4601−4612.
(55) Benesi, H. A.; Hildebrand, J. H. A Spectrophotometric Investigation of the Interaction of Iodine with Aromatic Hydrocarbons. *J. Am. Chem. Soc.* **1949**, *71*, 2703−2707.
(56) Kuntz, I. D., Jr; Gasparro, F. P.; Johnston, M. D., Jr; Taylor, R. P. Molecular interactions and the Benesi-Hildebrand equation. *J. Am. Chem. Soc.* **1968**, *90*, 4778−4781.
(57) Chakkamalayath, J.; Martin, L. E.; Kamat, P. V. Extending Infrared Emission via Energy Transfer in a CsPbI3-Cyanine Dye Hybrid. *J. Phys. Chem. Lett.* **2024**, *15*, 401−407.
(58) Hofmann, F. J.; Bodnarchuk, M.; Dirin, D. N.; Vogelsang, J.; Kovalenko, M. V.; Lupton, J. M. Energy transfer from perovskite nanocrystals to dye molecules does not occur by FRET. *Nano Lett.* **2019**, *19*, 8896−8902.
(59) Hofmann, F. J.; Bodnarchuk, M. I.; Protesescu, L.; Kovalenko, M. V.; Lupton, J. M.; Vogelsang, J. Exciton Gating and Triplet Deshelving in Single Dye Molecules Excited by Perovskite Nanocrystal FRET Antennae. *J. Phys. Chem.Lett.* **2019**, *10*, 1055−1062.
(60) Gallagher, S.; Kline, J.; Jahanbakhshi, F.; Sadighian, J. C.; Lyons, I.; Shen, G.; Hammel, B. F.; Yazdi, S.; Dukovic, G.; Rappe, A. M.; et al. Ligand Equilibrium Influences Photoluminescence Blinking in CsPbBr3: A Change Point Analysis of Widefield Imaging Data. *ACS Nano* **2024**, *18*, 19208−19219.
(61) Kay, E. R.; Lee, J.; Nocera, D. G.; Bawendi, M. G. Conformational Control of Energy Transfer: A Mechanism for

https://doi.org/10.1021/acs.jpcc.5c00337
J. Phys. Chem. C 2025, 129, 4134−4145

Biocompatible Nanocrystal-Based Sensors. *Angew. Chem., Int. Ed.* **2013**, *52*, 1165−1169.

https://doi.org/10.1021/acs.jpcc.5c00337
J. Phys. Chem. C 2025, 129, 4134−4145